O. Schlömer[1], and J. Herget[1]

[1]Department of Geography, University of Bonn, Germany

Corresponding author: Oliver Schlömer (oschloem@uni-bonn.de)

Key Points:

- Local scouring at boulder-like obstruction occurs predominantly on the rising limb of a hydrograph at comparable shallow flow depth
- Irrespective of hydrograph shape more than 70 percent of the final dimensions are attained in less than 10 percent of hydrograph duration
- Sediment supply induced by high flow intensity at peak flow refilled the local scour hole irrespective of hydrograph shape

This manuscript is the companion to:

*Schlömer, O., & Herget, J. (2021): Flume Experiments on the Geometry of Local Scour Holes at Boulder-Like Obstacles during unsteady flow conditions: Part II: - Enlargement Processes and the Impact of Hydrograph Chronology (*submitted to WRR*)*

Abstract

Local scouring is a complex phenomenon that is well studied at bridge piers while less attention is given to the time-dependent evolution of local scour holes at natural instream obstacles like boulders. This specifically applies to changing hydraulic boundary conditions at the obstacle in course of flood hydrographs while physical modelling in flumes offers the advantage that hydraulic boundary conditions can be systematically varied. This first companion paper yields novel experimental data on the impact of hydrograph shape and flow intensity on local scour hole formation and dynamics at boulder-like obstructions. Experimental results revealed that (1) intense incision and enlargement of local scour holes occurs on the rising limb irrespective of hydrograph shape at shallow flow depth that was comparable to the size of the obstacle while the impact of peak flow was negligible due to submergence of the obstacle. (2) Sediment supply due to general mobilization at high flow intensities partially refilled the emerging local scour holes and reduced the size of the geometrical length scales. (3) Two temporal stages of local scouring could be modelled based on statistical analysis of geometrical relations (depth to length, and depth to width) in time that were consistent to prior observations on constant hydraulic boundary conditions. This contribution improves the understanding of local scouring at boulder-like obstacles exposed to hydrographs while it is speculated that the identified length and time scales may be utilized for hydraulic interpretation at field condition.

Plain Language Summary

Local scour holes are structures related to obstructions like bridge piers or boulders that are exposed to flowing water. Scour holes emerge due vortices in the vicinity of the obstacle that mobilize sediment. Although the formation of local

scour holes at bridge piers is well studied because of safety problems, there is scarce knowledge on local scouring at natural obstacles in rivers like boulders. This specifically applies to the dynamic of scour hole formation under varying flow depth and flow velocity which is typically for floods. Here we present the results of a laboratory study on local scouring at boulder-like obstacles exposed to idealized floods of different shape, duration, and intensity. The results revealed that local scouring is a rapid process in time while the scour dynamic is intense for shallow flow depth that is comparable to the size of the boulder-like obstacle for the beginning stage of a flood. The peak of a flood had only a negligible impact on local scouring as the boulder-like obstacle was underwater. We suggest that local scour holes found at boulders in the field may be used for the temporal interpretation of the beginning stage of a flood.

1 Introduction

The phenomenon of local scouring emerges due to three-dimensional turbulent vortices generated by instream obstacles (natural or artificial) that obstruct and split the approaching current and induce sediment mobilization in its vicinity that causes an upstream crescentic local scour hole that laterally surrounds the obstacle, and a dune-like sediment accumulation in the downstream wake. As illustrated in Figure 1a, the local scour hole is an depression that can be approximated as inverted frustum-cone which is characterized by certain geometrical length scales, including scour hole depth at the obstacle front (d_s) measured from the undisturbed upstream bed; scour hole frontal length (l_s) in the plane of symmetry to the incoming flow, measured from the obstacle frontal face to the upstream edge of the scour hole, and scour hole frontal width (w_s) measured perpendicular to the direction of incoming flow form the lateral edges of the scour hole at the obstacle frontal face (Euler & Herget 2012). The topography is consistent and comparable across spatial scales from small scale laboratory (10^{-2} m) to local scour holes at boulder (10^{1} m) (Schlömer et al. 2021). Local scour holes at boulders are transient in the sense that they persist as long as the obstacle that creates them (Figure 1b).

Local scouring can be interpreted as the result of a complex two-phase flow involving water and sediment (Radice et al. 2009), that is controlled by different extrinsic and intrinsic environmental boundary conditions comprising (1) flow conditions, (2) sediment characteristics, (3) properties of the obstacle, and (4) time (Breusers & Raudkivi 1991; Melville & Coleman 2000; Schlömer et al. 2020). Hence, laboratory investigation of local scouring in a physical model (i.e. flume) offers the advantage that boundary conditions can be varied systematically while morphodynamics and flow structures can be analyzed and measured.

Traditionally, flow structures around instream obstacles and the formation of local scour holes is relevant to different scientific disciplines in Earth-science and hydraulic engineering. In hydraulic engineering the aim is to estimate equilibrium d_s (i.e. maximum scour depth that is likely after a prolonged exposure to steady flow) as length scale that is used in the design practice and directly comparable to the foundation depth of technical infrastructure like bridge piers

and abutments (Ettema et al. 2011; Pizarro et al. 2020). Equilibrium d_s is reached asymptotically in time, typically in order of days for non-cohesive alluvial sediment (i.e. sand and gravel) (Kothyari et al. 1992; Melville & Chiew 1999; Simarro et al. 2011; Oliveto & Hager 2002). Thus, equilibrium d_s is physical modelled for steady (peak) discharge of a given return period, typically 100 – 200 years, that at least last as long as the duration to reach equilibrium d_s (Manfreda et al. 2018; Tubaldi et al. 2017).

However, natural floods are characterized by unsteady discharge (i.e. velocity and flow depth at any fixed point in space varying over time) expressed as hydrographs of different shape which depends on rainfall intensity, catchment characteristics, and others (Rodríguez-Iturbe & Valdés 1979). The shape determines the time to peak discharge (Herget et al. 2015; Rushmer 2007; Collischonn et al. 2017) and can be operationalized by the skewness (i.e. duration of rising limb relative to falling limb), while for peak discharge high flow intensity (i.e. mean approach flow velocity relative to threshold velocity for general sediment movement) is supposed to induce sediment transport so that life-bed conditions prevail. For floods with minor intensity, clear-water conditions might prevail that favor the monotonously increase of local scour depth, whereas for major flood events live-bed conditions and sediment input into the local scour hole result in refilling mechanisms of the local scour hole (Pizarro & Tubaldi, 2019).

Concerning local scouring it is noted that except for large lowland rivers flood hydrographs might be typically shorter than the time to reach equilibrium, while subsequent floods might produce ongoing local scouring (Link et al. 2017). Recently, experimental studies have investigated the impact of flow variability onto the time evolution of local scouring at emergent bridge piers and its implication for the prediction of equilibrium d_s (Bombar 2020; Chang et al. 2004; López et al. 2014; Pizarro et al. 2017; Hager & Unger 2010; Link et al. 2020). For these conditions it is found that the rising limb and peak flow have the strongest impact onto local scouring while maximum d_s after the hydrographs is usually smaller than equilibrium d_s associated to the corresponding peak discharge and also the time to reach maximum d_s is reached usually smaller than the flood duration (Gjunsburgs et al. 2010; Tabarestani & Zarrati 2017; Link et al. 2017).

However, at natural obstacles (i.e. solitary boulders) hydrographs cause significantly different hydrodynamic conditions that can result in emergent conditions during lower flows (some portion of the obstacle protrudes above the water surface) and submerged conditions at higher flows (the obstacle occupies only the lower portion of the flow) (Euler et al. 2017; Shamloo et al. 2001). Although, the spatio-temporal evolution of local scouring at boulder-like obstructions is experimentally modelled for long lasting steady discharge of different flow intensities (Schlömer et al. 2021), no experimental data on the impact of hydrographs on the time evolution of geometrical relations of local scour holes at boulder-like obstructions is available. In particular, this is true for flash flood hydrographs typically for ephemeral dryland rivers (Reid et al. 1998; Powell 2009) where preserved local scour holes at boulders can be found (Figure 1b). According to

Alexander and Crooker (2016) a flash flood is characterized by flow of water that arrives suddenly at a fixed point, changes quickly in velocity and water depth, and lasts a short time.

Thus, the present study experimentally investigates the impact of hydrographs of different shape, varying duration, and different intensity onto local scouring at boulder-like obstacles and implications for the geometrical relations of the local scour hole (i.e. d_s/l_s and d_s/w_s) in time. Within this context, the objective of the contribution is not to derive a predictive equation for local scouring during hydrographs, but to:

1. Analyze the geometry of local scour holes for unsteady discharge in time by a systematic laboratory flume study.
2. Evaluate the consistency of prior observations on the evolution of geometrical relations of the local scour hole in time for different hydrograph scenarios.

An improved understanding of the geometry of local scour holes in time can therefore be auxiliary to (a) refine existing procedures to estimate parameters (e.g. duration) of past flood events at field conditions (Herget et al. 2013) and (b) estimate the spatial extent of countermeasure for local scour protection at technical infrastructure.

This study is related to a companion that evaluates the impact of hydrographs and discharge chronologies onto the enlargement processes and resulting geometry of local scour holes at boulder-like obstructions (Schlömer& Herget, 2021). For both contributions a process-focused physical model approach was chosen that reproduces processes and resulting morphologies. The hydrographs were modelled upon dimensionless parameters, but do not represent a specific natural prototype. The time-series data on local scour hole geometry is utilized by statistical and regression analysis.

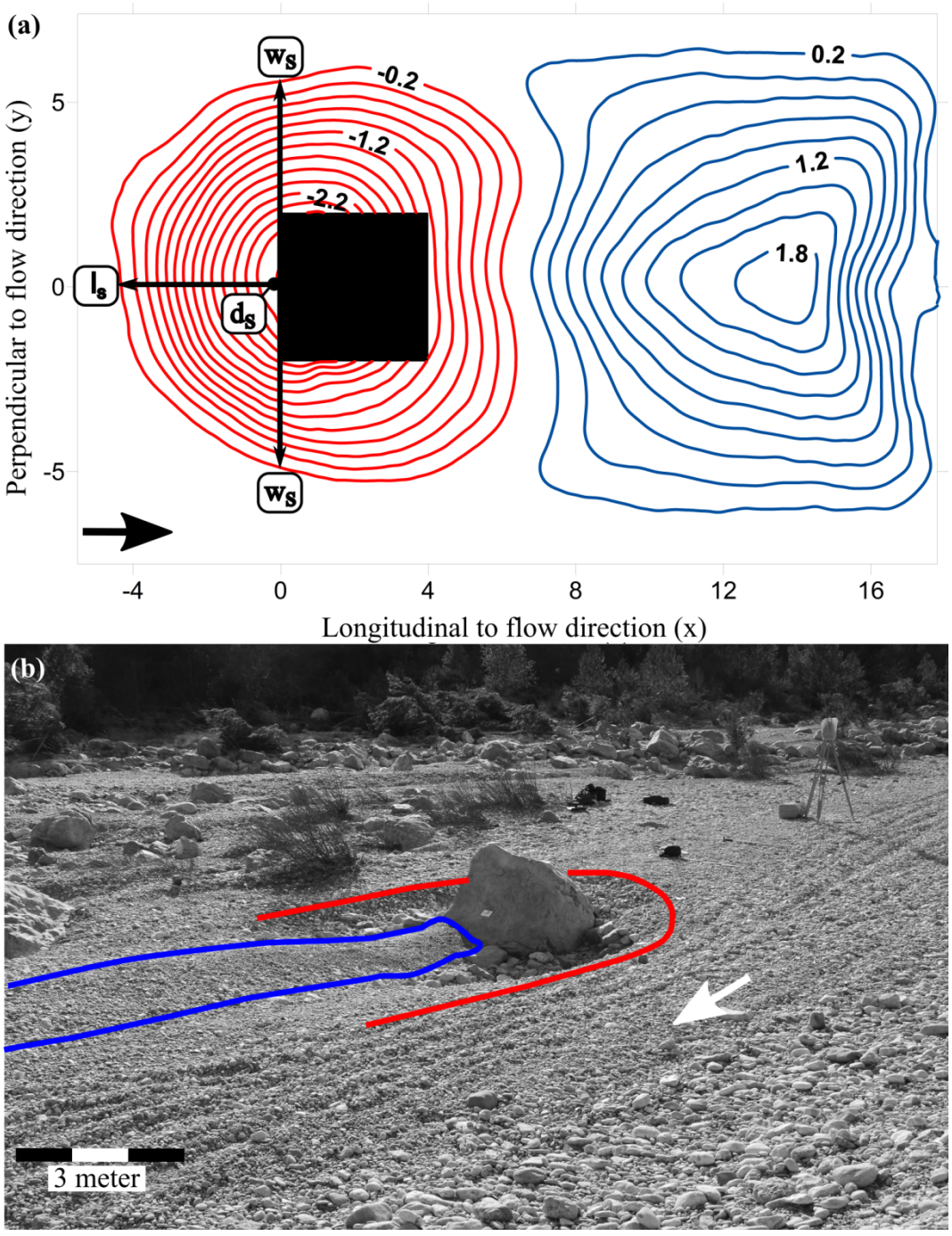

Figure 1. (a) Plan view of a local scour hole at a cuboid obstacle at laboratory scale (cm) indicating local scour hole (red isolines) and sediment ridge (blue iso-

lines). (b) Local scour hole and sediment ridge at a tilted boulder in ephemeral Rambla de la Viuda (2019, NE Spain). Arrows indicates direction of flow.

1.1 Local Scouring in Time

Local scour holes originate from deformations of the approaching flow field in the vicinity of an obstacle that result in the following processes (1) contradiction of streamlines lateral to the obstacle, inducing higher flow velocities; (2) formation of a jet-like downflow at the obstacle front due to pressure gradient; (3) formation of unsteady turbulent necklace-like vortical structures at the obstacle base commonly referred as horseshoe vortex system (HV) (Escauriaza & Sotiropoulos 2011; Kirkil & Constantinescu 2010; Radice & Tran 2012; Chen et al. 2017). Processes (1) to (3) amplify bed shear stress by one order of magnitude larger than those generated by classical turbulent shear mechanism in the approach flow inducing sediment mobilization even if sediment transport in the undisturbed approaching flow is absent and clear-water conditions prevail (i.e. mean approach velocity $<$ threshold velocity for general sediment movement) (Li et al. 2018; Link et al. 2012). The HV is the main driver of incision and spatial enlargement as it subsides into the bottom local scour where sediment is picked up and transported into the downstream wake by saltation and rolling (Chen et al. 2019; Dargahi 1990) The enlargement of the scour hole in length (l_s) and width (w_s) is forced by the depth-incision as steepening of the scour hole slopes causes mass movements into the local scour hole. The depth-incision is a non-linear process in time because the HV expands in diameter and the shear stress beneath the vortices decreases and equilibrium condition is approached when the HV is no longer capable of removing sediment (Kothyari et al. 1992). From laboratory data at clear-water conditions it is well established that 80% of equilibrium d_s is developed within only 5-40% of the time to equilibrium that is obtained after several days, mainly depending on approach flow velocity (Melville & Chiew 1999). However, the interpretation of equilibrium d_s, i.e. a scour depth that does not increase further in time and is close to its ultimate size is rather subjective as it has implications for the design of experiments (Simarro et al. 2011).

From laboratory runs on long lasting constant peak discharge (5750 min) and for a given sediment and obstacle size, Schlömer et al., (2020b) found that the size of l_s and w_s scales with d_s and elapsed time (t), and only indirect with the actual flow conditions. Depth-incision was intense for $t \sim 240$ min and considerably eased afterwards while the local scour hole remained active and slight enlargement occurred for l_s and w_s for $t > 240$ min so that distinct geometrical relations (i.e. d_s/l_s and d_s/w_s) in time could be described.

For live-bed conditions and sediment transport in the undisturbed flow, equilibrium d_s is reached when the average of sediment transported into the scour hole is equal to the sediment transported out of the local scour hole due to the HV (Sheppard & Miller 2006). Due to the high flow velocity the scour incision in time is faster.

2. Experimental Design

As briefly anticipated in the introduction, local scour incision at a solitary boulder-like obstacle located in a straight, moderately sloped channel and embedded in non-cohesive sediment functionally depends on a set of dimensionless control parameters that are derived upon principles of the Buckingham Π theorem (Schlömer et al. 2020):

$$d_s/L_o = f\,(d_w/L_o,\ U_m/U_c,\ Re_o,\ L_o/B,\ Sh,\ Mb,\ L_o/D_{50},\ _G,\ d_{sed}/L_o,\ t/t_e) \quad (1)$$

where d_w/L_o is the submergence ratio (d_w = flow depth [L] and L_o = effective obstacle size ${h_o}^{2/3}\ {w_o}^{1/3}$ [L], with h_o = obstacle height [L] and w_o = obstacle width [L], U_m/U_c is flow intensity (U_m = mean approach velocity [LT^{-1}] and U_c = critical mean approach velocity for entrainment of sediment [LT^{-1}]), Re_o is the obstacle Reynolds number ($U_mL_o/$, with = kinematic viscosity of water [L^2T^{-1}]), L_o/B is the blockage ratio (with B = channel width [L]), Sh [-] is an indicator for the hydrodynamic shape of the obstacle, Mb [-] is an indicator for the mobility of boulder-like obstruction due to tilting into the local scour hole, L_o/D_{50} is the relative sediment coarseness (D_{50} = median diameter of the bed sediment [L]), $_G$ is the sorting of sediment (${D_{84}/D_{16}}^{1/2}$ [-]), d_{sed}/L_o is the relative thickness of the alluvial layer (d_{sed} = thickness of the alluvial layer in which the obstacle is embedded [L]), and t/t_e is the time scale of local scouring. Each term in equation (1) is measurable or readily simulated with the current state-of-the-art technology for measuring or modelling three-dimensional flows and local scouring.

Submergence ratio (d_w/L_o) is a particularly important boundary control parameter of local scouring, as boulder-like instream obstacles are affected by different water levels (Papanicolaou et al. 2010). For $d_w/L_o = 1$ a high pressure gradient at the obstacle front is present, creating an intense downflow and strong HV at the obstacle base while this effect gradually weakens for $d_w/L_o > 1.1$ and higher d_w as the obstacle submerges (Schlömer et al., 2020a). Moreover, for a given sediment size U_c depends on d_w (Simarro et al. 2007). Thus, d_w, U_m, U_c, and t are the particular variables of interest for modelling varying discharge in the course of a hydrograph and evaluating its impact on local scouring. Within this context, it is worthwhile to mention that neither hydrographs nor obstacle dimensions were scaled to a prototype and the flume experiments are interpreted as unscaled process-focused physical models (Baynes et al. 2018).

2.1 Flume Set-Up

Experiments were conducted in a in a 5 m long, 0.32 m wide, and 0.27 m deep straight rectangular flume with fixed slope (0.003 m m^{-1}) entirely filled with a 5.5 cm thick layer (d_{sed}) of uniform ($_G < 1.3$) sand with median grain diameter (D_{50} = 0.75 mm). D_{16} and D_{84} were 0.61 mm and 0.89 mm, respectively.

Discharge was controlled by a recirculating pump (Lowara FCE-series®) regulated by two cone valves and measured by a magnetic-inductive discharge meter (Schwing MS 1000®, accuracy ± 1% of actual discharge). Flow depth (d_w) was

adjusted by a tail-gate at the downstream end of the flume to enable pseudo-uniform flow (Hager & Hutter 1984) within the working section of the flume (~ 2.7 m downstream of the inlet).

A cube ($L_o = 3$ cm) was used to mimic an angular instream boulder-like obstacle that was mounted to the flume bottom within the working section in the plane of symmetry to prevent tilting into the scour hole and to minimize sidewall effects (Nakagawa & Nezu 1993). Blockage ratio (L_o/B, with B = flume width) and relative sediment coarseness (L_o/D_{50}) were designed to satisfy critical thresholds for the onset of local scouring, i.e. $L_o/D_{50} > 8$ (Lee & Sturm 2009), and $L_o/B < 0.6$ (Williams et al. 2019). Thus, neglecting viscous effects (Manes et al. 2018) equation (1) reduces to

$$d_s/L_o = f\,(d_w/L_o,\, U_m/U_c,\, t/t_e) \quad (2)$$

where t_e is interpreted as the overall duration of laboratory hydrograph.

2.2 Laboratory Hydrographs

The laboratory hydrographs were modelled following a quasi steady approach and the principle of a stepped hydrograph (Link et al. 2017; López et al. 2014), i.e. a sequence of constant discharges acting during defined intervals which is commonly used to simulate varying discharge in flumes (Mao 2012; Waters & Curran 2015). The stepped hydrographs were constructed with 13 intervals of constant discharge: six on the rising limb, one at peak flow, and six on the falling limb for three experimental series (A, B, C) that had different overall durations (t_e). For series A t_e was 480 min, for series B t_e was 210 min, and for series C t_e was 120 min.

For each experimental series the duration of rising limb (t_r), falling limb (t_f), and peak flow (t_{peak}) was variable to generate four, relatively simple shaped single peaked hydrographs (Figure 2a-d). For the symmetrical hydrograph ($t_r/t_f = 1$; $t_r/t_e = 0.5$) of series A each interval lasted 37 min on t_r and t_f while t_{peak} lasted 36 min;

on the positive skewed hydrograph ($t_r/t_f < 1$, here = 0.28; $t_r/t_e = 0.21$) the intervals on t_r and t_f lasted 17 min and 60 min, respectively, while t_{peak} lasted 18 min;

on the flash flood hydrograph ($t_r/t_f \ll 1$, here = 0.08; $t_r/t_e = 0.075$) the intervals on t_r and t_f lasted 6 min and 73 min, respectively, while t_{peak} lasted 6 min;

on the negative skewed hydrograph ($t_r/t_f > 1$, here = 3.53; $t_r/t_e = 0.75$) the intervals on t_r and t_f lasted 60 min and 17 min, respectively, while t_{peak} lasted 18 min and $t_e = t_r + t_{peak} + t_f$.

Additionally, three experiments with long lasting, constant peak flow rate over $t_e = 480$ were performed for three different hydraulic scenarios (Figure 2e).

Series B experiments (t_r = 1 min - 30 min, t_f = 4 min – 33 min) were designed for the positive skewed, negative skewed, and flash flood hydrograph to extent

the degree of skewness of (t_r/t_f = 0.05, 0.14, and 7.06) (Figure 2f).

Series C experiments (t_r = 1 min - 15 min, t_f = 4 min – 18 min) were carried out for all four hydrographs to further evaluate the impact on time-dependent local scouring. At this, it is assumed that the number and duration of interval ensured that the stepped hydrographs realistically modeled the unsteady nature of a natural hydrograph (Waters & Curran 2015). In total 36 experiments at three different hydraulic scenarios (see next chapter) were conducted.

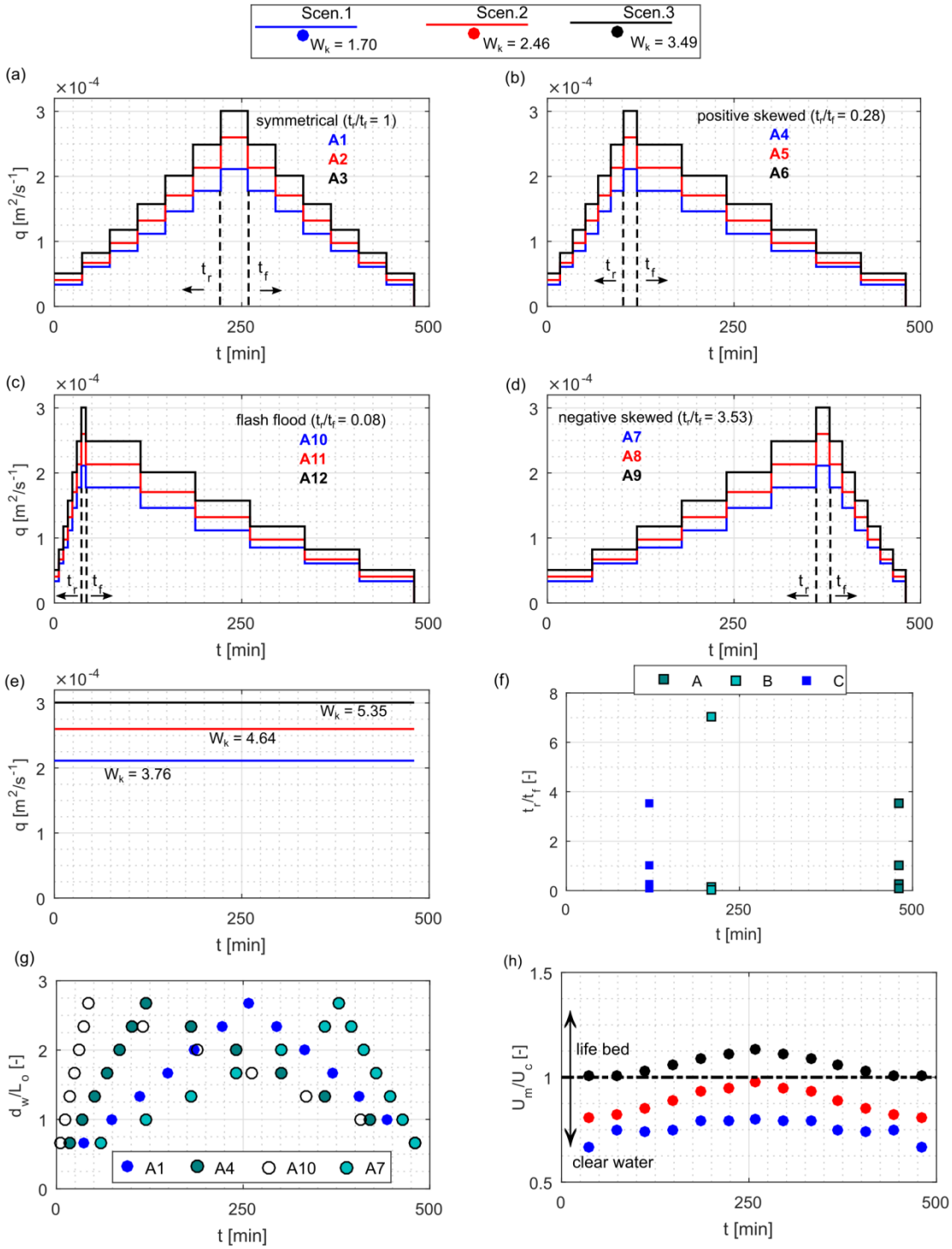
Scen.1
W_k = 1.70
Scen.2
W_k = 2.46
Scen.3
W_k = 3.49
(a)
symmetrical (t_r/t_f = 1)
A1
A2
A3
(b)
positive skewed (t_r/t_f = 0.28)
A4
A5
A6
(c)
flash flood (t_r/t_f = 0.08)
A10
A11
A12
(d)
negative skewed (t_r/t_f = 3.53)
A7
A8
A9
(e)
W_k = 5.35
W_k = 4.64
W_k = 3.76
(f)
A
B
C
t_r/t_f [-]
(g)
d_w/L_o [-]
A1
A4
A10
A7
(h)
U_m/U_c [-]
life bed
clear water
q [m^2/s^-1]
t [min]

Figure 2. Laboratory hydrographs for series A experiments (a-e) and hydraulic boundary conditions of experimental scenarios A, B, and C (f) skewness of hydrographs. (g) submergence ratio during hydrographs. h) flow intensity during hydrographs.

2.3 Hydraulic Conditions of Laboratory Hydrographs

Different unit discharges (q) on the intervals of the stepped hydrographs were generated by a variation of d_w and U_m (Table 1). The hydrograph started form a drained flume (i.e. no baseflow). On the rising limb, d_w was linearly increased from 2 cm at the first interval to 8 cm at peak flow (7^{th} interval) while on the falling limb d_w was decreased linearly to 2 cm again, producing emergent (d_w/L_o < 1) and submerged conditions ($d_w/L_o \gg 1$) at the obstacle during the hydrographs (Figure 2g). By increasing U_m for given d_w, different flow intensities (U_m/U_c) were created that distinguish between clear-water conditions (U_m/U_c 1, scenario 1 and 2), as well as live-bed conditions (U_m/U_c >1.01, scenario 3). For scenario 1 and 2, the peak flow intensity ($I_p = U_m/U_c$) was 0.8 and 0.98, respectively, while for scenario 3 I_p was 1.13 and the sediment was solely transported as bed load (i.e. lower stage plane bed) For each d_w was set at U_m/U_c > 0.5 to guarantee local scouring (Chiew 1995) while the flow was subcritical (Figure 2h). For different d_w, U_c was by estimated by

$$U_c = 5.75\log_{10}(5.53d_w/D_{50})u_{c*} \quad (3)$$

where u_c* is the critical shear velocity [LT^{-1}] that was estimated by Melville and Coleman (2000)

$$u_c* = (0.0115+0.0125)D_{50}{}^{1.4} \ (0.1 \text{ mm} < D_{50} < 1 \text{ mm}) \quad (4)$$

Furthermore, the hydrographs were operationalized by calculating the dimensionless total flow work index, W_k as indicator for the magnitude (Waters & Curran 2015)

$$W_k = u_p{}^{*2} /(gd_w{}^3B) \quad (5)$$

where u_p* is the shear velocity [LT^{-1}] at peak flow (q_p), is the total volume of water under the hydrograph [L^3], and g is gravitational acceleration [LT^{-2}]

u_p* was estimated from semi-logarithmic velocity profiles (Bergeron & Abrahams 1992) measured from an acoustic Doppler velocimeter (ADV), yielding $W_k = 1.70$ for scenario 1, $W_k = 2.46$ for scenario 2, and $W_k = 3.49$ for scenario 3.

For the experimental runs on constant peak flow rate over t_e, W_k was estimated 3.76 for scenario 1, $W_k = 4.62$ for scenario 2, and $W_k = 5.35$ for scenario 3.

The hydrological conditions of the different hydrographs (i.e. no baseflow, relatively short duration) were designed to mimic scenarios possible occurring in ephemeral streams, although the hydrographs were not scaled (Camarasa-Belmonte & Segura 2001).

Table 1. Hydraulic boundary conditions of flow steps used to design hydrographs shown in Figure 2

	Scen. 1[a] W_k = 1.70	Scen. 2[b] W_k = 2.46	Scen. 3[c] W_k = 3.49					
Interval (n) [-]	d_w [m]	U_c[d] [ms^{-1}]	U_m [ms^{-1}]	q [m^{2}s^{-1}]	U_m [ms^{-1}]	q [m^{2}s^{-1}]	U_m [ms^{-1}]	q [m^{2}s^{-1}]
+ 13				10^{-5}		10^{-5}		10^{-5}
+ 12				10^{-5}		10^{-5}		10^{-5}
+ 11				10^{-5}		10^{-5}		10^{-4}
+ 10				10^{-4}		10^{-4}		10^{-4}
+ 9				10^{-4}		10^{-4}		10^{-4}
+ 8				10^{-4}		10^{-4}		10^{-4}
				10^{-4}		10^{-4}		10^{-4}

Note. [a] A/B/C 1, 4, 7, 10. [b] A/B/C 2, 5, 8, 11. [c] A/B/C 3, 6, 9, 12. [d] Equation (4)

2.4 Experimental Procedure

The experiments started at t = 0 min after adjusting d_w and q to the first interval of the hydrograph and introducing the obstacle in the working section to induce local scouring immediately. Between intervals on the rising limb the tailgate was raised 1 to 2 cm to interrupt local scouring while q was adjusted to the next interval. On the falling limb, first q was decreased while the tailgate was lowered to the corresponding d_w.

Dimensions of d_s, l_s, and w_s were measured with two LED-distance meters (Welotec® OWRB-series, accuracy ± 0.5 mm), measuring in longitudinal streamwise direction (i.e. x) and perpendicular to streamwise direction (y); and a laser distance meter (Baumer Electric® ODAM S14C, accuracy ± 1.5 mm) measuring in the vertical direction (z). The sensors were mounted on a traversing system on top of the flume operating in x/y –plane. For series A measurements of d_s, l_s, and w_s were sampled every third minute on each hydrograph step. For series B and C the measurement frequency was relaxed to one and two min, respectively, to generate sufficient data on each hydrograph step.

3. Results

The experimental dataset is accessible via the Havard dataverse repository:

https://doi.org/10.7910/DVN/EYQP2U.

3.1 Time Evolution of Local Scouring

Irrespective of experimental series, local scouring started immediately at t = 0.1 min at the lateral edges of the obstacle and rapidly merged to a local scour hole in front of the obstacle (t 1 min). Subsequently, the local scour hole deepened as well as lengthened and widened while the sediment ridge flattened, widened and elongated in downstream direction. The arrival of the flood front and the induced impulsive force at the obstacle frontal face did not alter the position of the obstacle.

For W_k = 1.70 local scouring was non-linear in time and characterized by a high rate of depth-incision for the beginning of experiment (t/t_e 0.1). The depth-incision eased afterwards and asymptotically reached its final value (d_{se}) at t_e, irrespective of experimental series and hydrograph shape (Figure 3). The enlargement of l_s and w_s towards their final values (i.e. l_{se}, w_{se}) at the end of the experiments was directly coupled to d_s as incision undermined the scour hole slopes and induced gravitational movements of sediment that caused and enlargement in local scour hole length and width irrespective.

At t/t_e = 0.1 and irrespective of the hydrograph shape, d_s already reached 76% of d_{se} while l_s and w_s reached 77% of their dimensions at t_e, respectively. At t/t_e = 0.4, d_s and l_s reached 96% and 97%, respectively, of their dimensions at t_e while w_s/L_o reached 94% of its dimensions at t_e. The non-linear evolution of local scouring was also present for the run on constant q_p at Wk = 3.76 (Figure 3m-o). At t/t_e = 0.1, d_s, l_s and w_s/L_o reached 78%, 85%, and 77%, respectively of their dimension at t_e For t/t_e = 0.4 already 98% (d_s), 96% (l_s), and 92% (w_s) of the dimensions at t_e were reached.

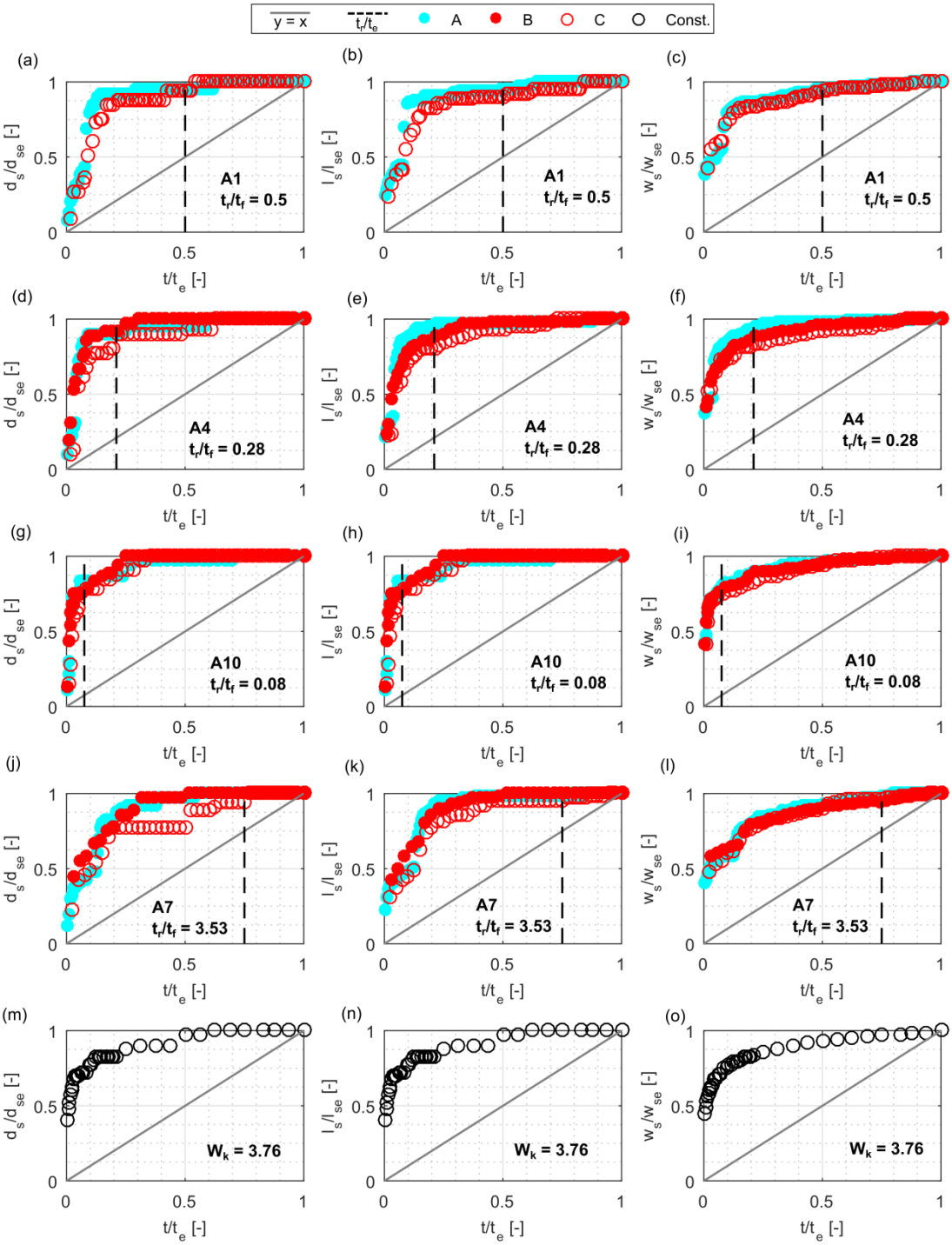
y = x
t_r/t_e
A
B
C
Const.
(a)
(b)
(c)
(d)
(e)
(f)
(g)
(h)
(i)
(j)
(k)
(l)
(m)
(n)
(o)
d_s/d_{se} [-]
l_s/l_{se} [-]
w_s/w_{se} [-]
t/t_e [-]
A1
t_r/t_f = 0.5
A4
t_r/t_f = 0.28
A10
t_r/t_f = 0.08
A7
t_r/t_f = 3.53
W_k = 3.76

Figure 3. d_s, l_s, and w_s in time for different hydrograph shapes of experimental series A, B, and C (a-l) and runs on constant q_p (m-o). Normalized by final size (d_{se}, l_{se}, and w_{se}) at t_e.

3.1.1 Hydrograph Shape

The asymptotical evolution of local scouring implies that substantial enlargement occurred during the rising limb (t_r) of the hydrograph prior to q_p (cf. dashed line in Figure 3)

Thus, skewness (t_r/t_f) of the hydrographs affected local scouring in time. For $t_r/t_f = 0.08$ at $W_k = 1.70$ (Figure 4g) 82% of d_s/L_o, l_s/L_o, and w_s/L_o at t_e were reached during t_r approaching q_b which corresponds to 7.5% of the duration of t_e. For $t_r/t_f = 3.53$ at $W_k = 1.70$ (Figure 4j) the geometrical length scales reached 99% of their dimensions at t_e on t_r which corresponds to 75% of the duration of t_e. This observation is supported considering the two extremums of the investigation (series B, $t_e = 210$ min). For $t_r/t_f = 0.05$, 69% of d_s/L_o, l_s/L_o, and w_s/L_o at t_e were reached during t_r while for $t_r/t_f = 7.06$, 99% of d_s/L_o, l_s/L_o, and w_s/L_o at t_e were reached during t_r and prior to reach q_p. However, it becomes obvious that especially the initial intervals during t_r significantly impacted the local scouring process as indicated by superposition that were pronounced on the symmetrical and negative skewed hydrographs (cf. Figure 4a and j, indicated by arrows). These initial intervals correspond to conditions for which $d_w/L_o = 1$.

It is worth to mention that for given W_k the dimensions of d_s/L_o, l_s/L_o, and w_s/L_o at t_e were approximately similar irrespective of hydrograph shape. Comparing different hydrograph shapes the relative standard deviations for d_s/L_o, l_s/L_o, and w_s/L_o at $W_k = 1.70$ was 0.0282, 0.0136, and 0.0329, respectively while for $W_k = 2.46$ and 3.49 the relative standard deviations for d_s/L_o, l_s/L_o, and w_s/L_o at different hydrographs were slightly larger (~ 0.0395). However, it becomes obvious that the shape of the hydrograph of a given magnitude (i.e. W_k) is not influencing the size of the geometrical length scales of the local scour hole at the end of the experiments.

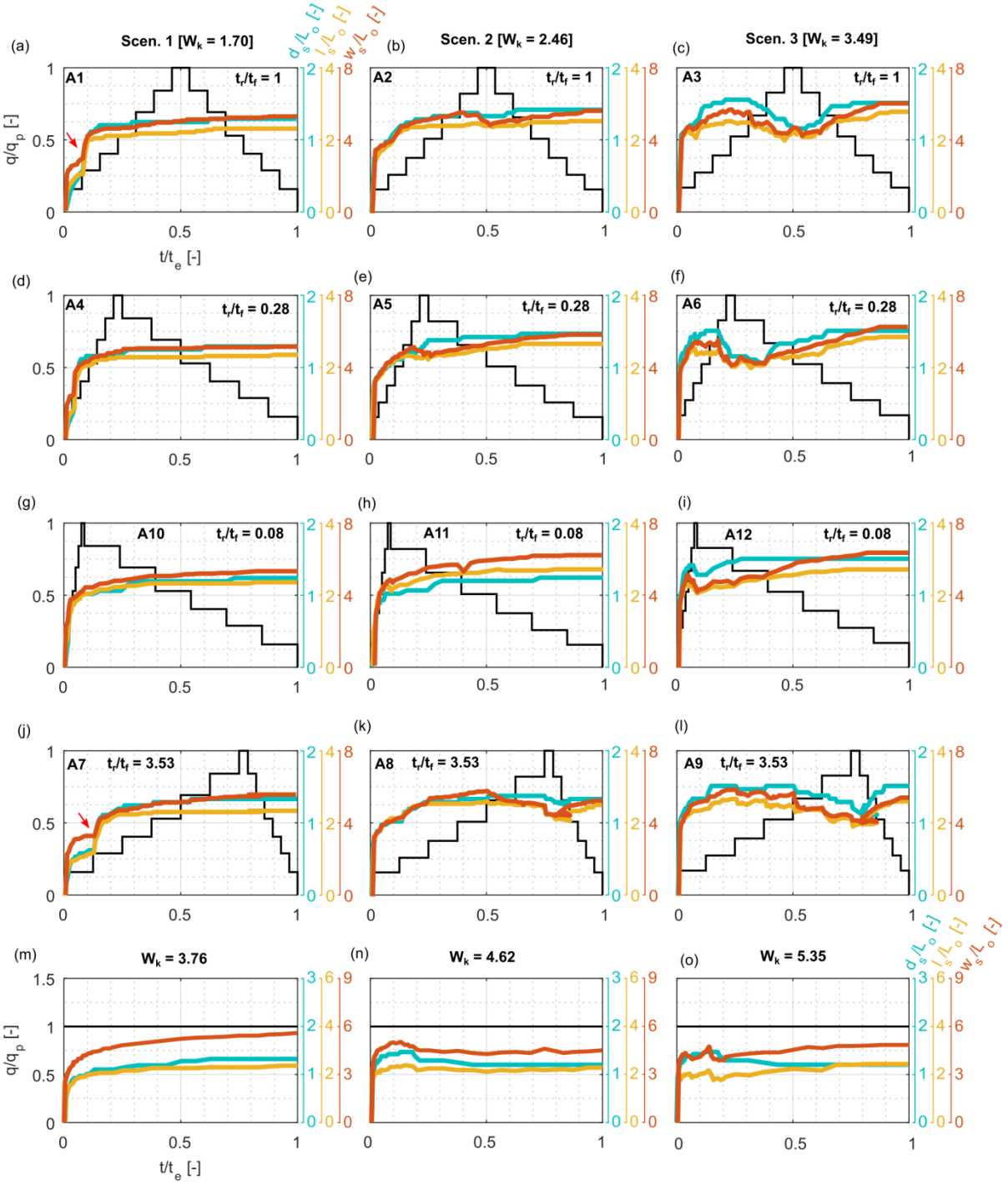
(a)
Scen. 1 [W_k = 1.70]
(b)
Scen. 2 [W_k = 2.46]
(c)
Scen. 3 [W_k = 3.49]
d_s/L_o [-]
l_s/L_o [-]
w_s/L_o [-]
A1 t_r/t_f = 1
A2 t_r/t_f = 1
A3 t_r/t_f = 1
(d)
(e)
(f)
A4 t_r/t_f = 0.28
A5 t_r/t_f = 0.28
A6 t_r/t_f = 0.28
(g)
(h)
(i)
A10 t_r/t_f = 0.08
A11 t_r/t_f = 0.08
A12 t_r/t_f = 0.08
(j)
(k)
(l)
A7 t_r/t_f = 3.53
A8 t_r/t_f = 3.53
A9 t_r/t_f = 3.53
(m)
W_k = 3.76
(n)
W_k = 4.62
(o)
W_k = 5.35
q/q_p [-]
t/t_e [-]

Figure 4. Trajectory of d_s, l_s, and w_s in time for series A differentiated by hydrograph shape (a-l), flow work index (W_k), and runs on constant q_p (m-o). Normalized by L_o.

3.1.2 Overall Duration

For series B and C t_e was reduced to 44% and 25% compared to the duration of series A experiments, respectively, which had an impact on the sizes of d_s/L_o, l_s/L_o, and w_s/L_o at t_e.

For series B ($W_k = 1.70$) the geometrical length scales at t_e were on average 4% smaller compared to series A while for series C ($W_k = 1.70$) d_s/L_o, l_s/L_o, and w_s/L_o were on average 12% smaller compared to series A at t_e irrespective of hydrograph shape.

Although the non-linear evolution in time was not different, the reduced overall duration of the experiments affected local scouring in time. For series C ($W_k = 1.70$) at $t/t_e = 0.1$, d_s/L_o reached 64% of its dimension at t_e while l_s/L_o reached 61%, and w_s/L_o reached 70% of its dimensions at $t_e = 1$. For $t/t_e = 0.4$, d_s/L_o reached 89% of its dimension at t_e while l_s/L_o reached 92%, and w_s/L_o reached 90% of its dimensions at t_e irrespective of hydrograph shape. For increasing W_k the sizes of d_s/L_o, l_s/L_o, and w_s/L_o at t_e increased simultaneously while the order of difference in between series A, B, and C scaled approximately (Figure 5a-l).

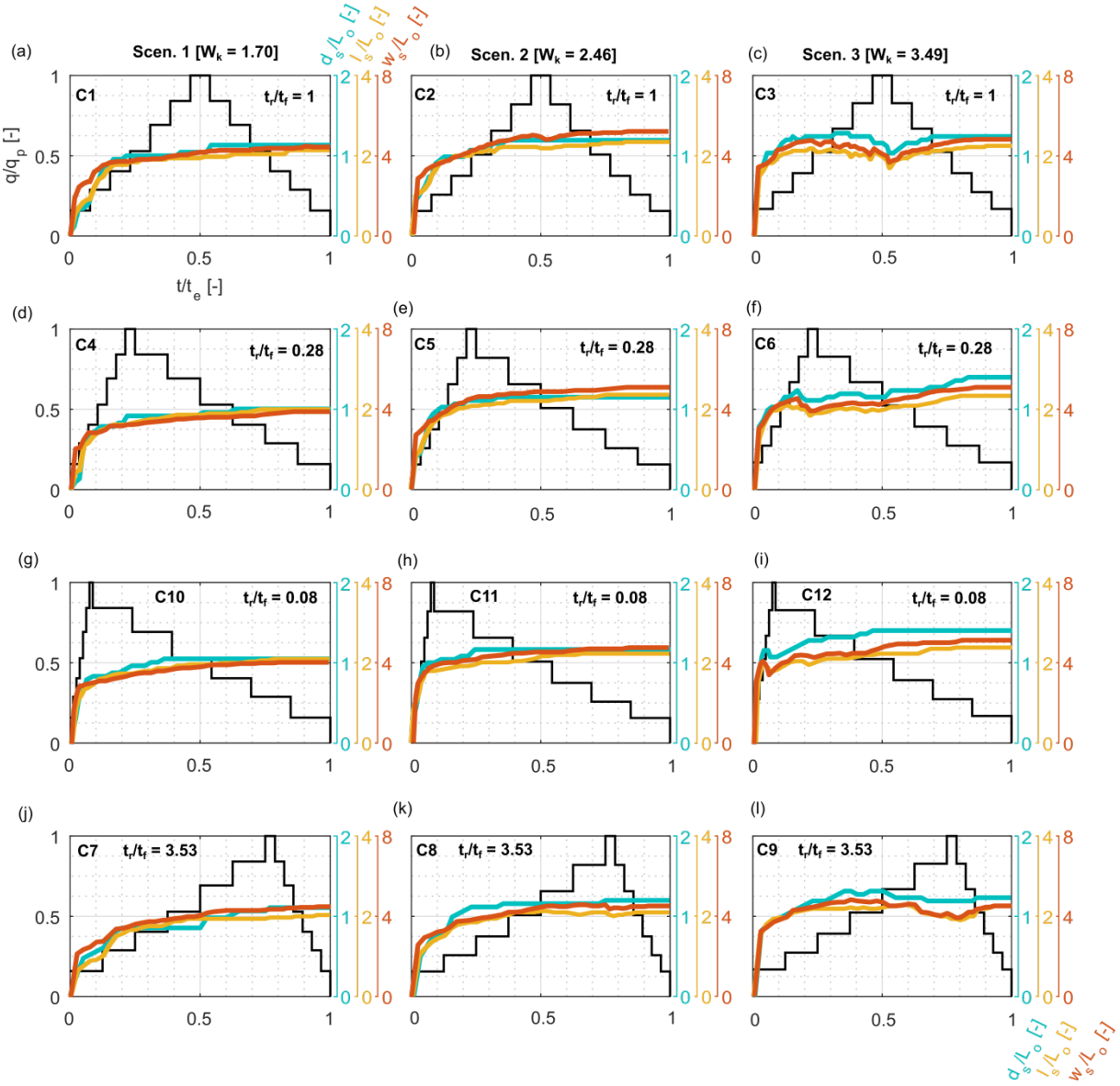

Figure 5. Trajectory of d_s, l_s, and w_s in time for series C differentiated by hydrograph shape (a-l), flow work index (W_k), and runs on constant q_p (m-o). Normalized by L_o.

3.2 Flow Intensity

The non-linear evolution of local scouring did not differ for increasing W_k and U_m/U_c while the size of d_s/L_o, l_s/L_o, and w_s/L_o on t_r increased irrespective of hydrograph shape. However, for $W_k = 3.49$ the flow intensity (U_m/U_c) on

each step was > 1 so that general bed load transport prevailed during the experiments indicated by downstream migrating bed load sheets. At peak flow, the high flow intensity (I_p = 1.13) caused passages of bed load sheets in the scour hole that reduced the geometrical length scales irrespective of hydrograph shape by refilling and partial burying the local scour hole (Figure 4 and 5c, f, l, i). A similar evolution took place for W_k = 2.46 and I_p = 0.98 where sediment < D_{50} was already transported as bed load (Figure 4 and 5b, e, h, k). However, after the peak flow local scouring occurred also on the falling limb of the hydrographs for W_k = 2.46 and 3.49, respectively, so that d_s/L_o, l_s/L_o, and w_s/L_o reconstitute to sizes comparable to pre-peak flow conditions as the sediment supply into the local scour hole mitigated. For the runs on constant peak flow at W_k = 4.62 and 5.35, respectively, the sediment supply due to live-bed conditions lead to fluctuating variations of d_s/L_o, l_s/L_o, and w_s/L_o in time (Figure 4n, o). Thus, data on the geometrical length scales at t_e is rather undifferentiated. While d_s/L_o was larger for W_k = 5.35 compared to W_k = 3.76 (Figure 6m), w_s/L_o was smaller (Figure 6o).

However, the shape of the hydrograph affected at live-bed conditions influenced the size of the geometrical length scales at t_e. For W_k = 3.49 l_s/L_o and w_s/L_o were maximized for the flash flood and the positive skewed hydrograph while d_s/L_o was equal in series A and C (Figure 4d-g). For series A l_s/L_o and w_s/L_o were 4%, respectively 17% larger for the flash flood hydrograph compared to the negative skewed hydrograph (Figure 6l) while for series C l_s/L_o and w_s/L_o were 8%, respectively 15% larger as the time of sediment supply into the local scour hole was considerable shorter illustrating the complex interactions between flow and sediment in time.

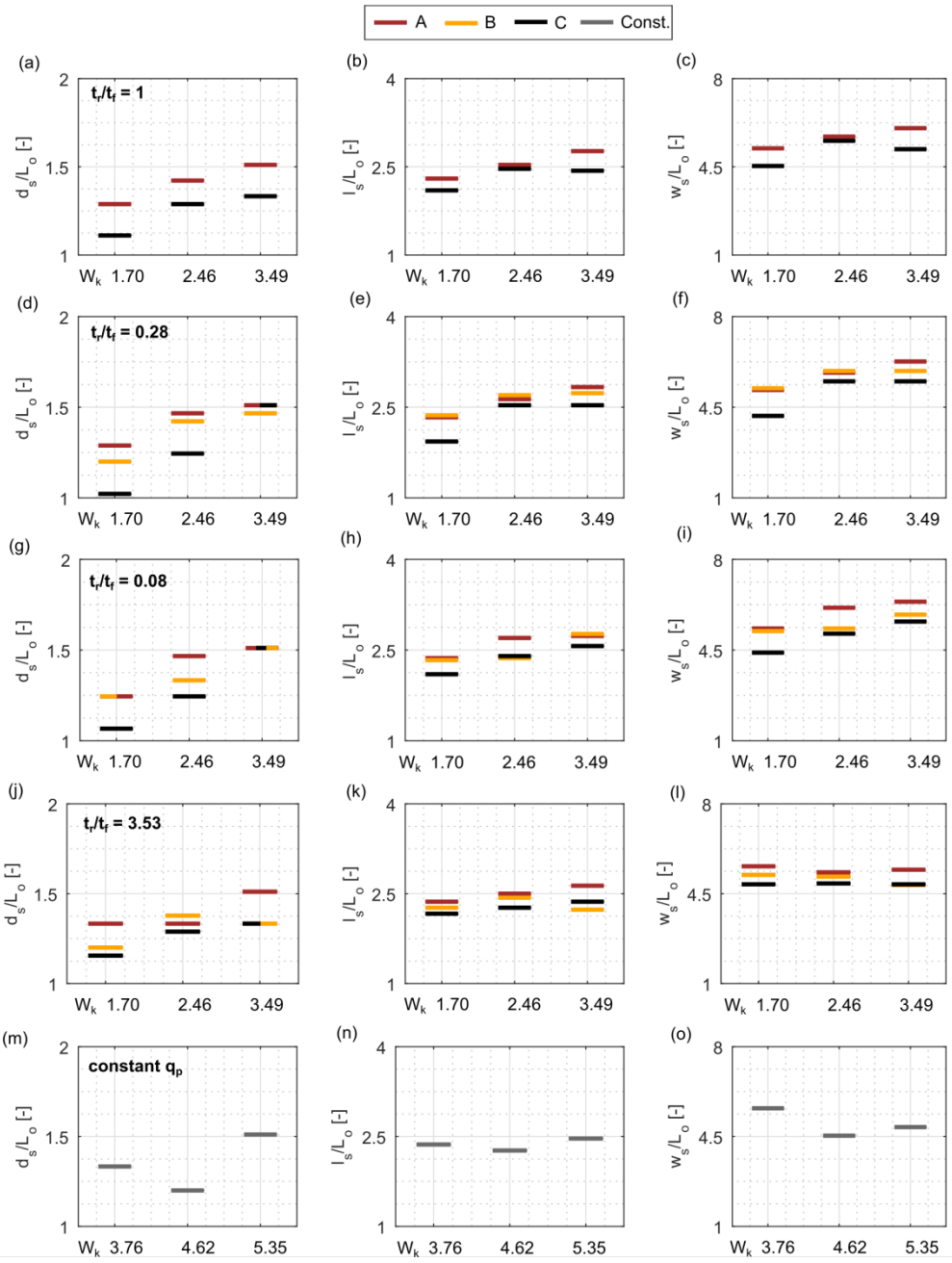

Figure 6. Normalized geometrical length scales of the local scour hole at t_e for different hydrograph shapes of experimental series A, B, and C (a-l) and runs on constant q_p (m-o) at different W_k.

3.3 Geometrical Relation

Figure 7 shows the geometrical relations (i.e. d_s/l_s and d_s/w_s) of the local scour hole for series A, B, and C at $W_k = 1.70$ plotted against t/t_e on a semi-logarithmic scale. Irrespective of hydrograph shape it becomes obvious that the geometrical relations are not constant over time but show a piecewise linear pattern while there is no obvious discrepancy for d_s/l_s and d_s/w_s for different experimental series as the relation over time collapse into common form. It is composed of

1. considerable enlargement in d_s/l_s and d_s/w_s for the beginning of local scouring as d_s increased quicker than l_s and w_s, approaching a maximum value in d_s/l_s and d_s/w_s;
2. easing enlargement and decreasing tendency in d_s/l_s and d_s/w_s afterwards as scour incision relaxed and d_s matured to its finale size while slight enlargement in w_s occurred;

Quantitatively, the stages are separated by change points that mark instabilities in the slope coefficients (ß1) for the regression of d_s/l_s and d_s/w_s over t/t_e. To achieve stationarity as requirement for statistical modeling, d_s/l_s and d_s/w_s were de-trended by subtracting the mean as a statistically significant trend was present due to the time-series character of the data as a Mann-Kendall test revealed ($p < 0.001$).

The procedure maintained the positions of the instabilities in time that were determined by minimizing the sum of the residual error that returns significant changes in slope, not exceeding permissible and predefined thresholds (Killick et al. 2012).

For different hydrograph shapes at $W_k = 1.70$ the occurrence of change points in d_s/l_s over t/t_e slightly varied, ranging from $t/t_e = 0.0167$ at $t_r/t_f = 0.05$ – 0.08 to $t/t_e = 0.0563$ at $t_r/t_f = 3.53$ – 7.06. For d_s/w_s over t/t_e at the same hydrograph shapes the change points occurred at t/te = 0.0238 to 0.175. The change points in time are displayed as dashed lines in Figure 6 while for further analysis $t/t_e = 0.05$ (for d_s/l_s) and $t/t_e = 0.1$ (for d_s/w_s) are used.

In between the change points the slope coefficients were significantly different irrespective of hydrograph shape as proposed in (a) and (b) characterized by a steep slope before the change point while the slope is near zero or negative afterwards. The slope coefficients were estimated by generalized least squares and an autoregressive- moving average model (ARIMA) due to the autocorrelation of residuals.

At the change points the intercept (ß2) corresponded to the maximum value of d_s/l_s and d_s/w_s in t/t_e. For d_s/l_s, ß2 ranged from 0.53 at $t_r/t_f = 0.05$ – 0.08 to 0.56 at $t_r/t_f = 0.5$ while mean and median was 0.54. For d_s/w_s, ß2 ranged from 0.24 at $t_r/t_f = 0.05$ – 0.08 to 0.26 at $t_r/t_f = 0.5$ while mean and median was 0.25.

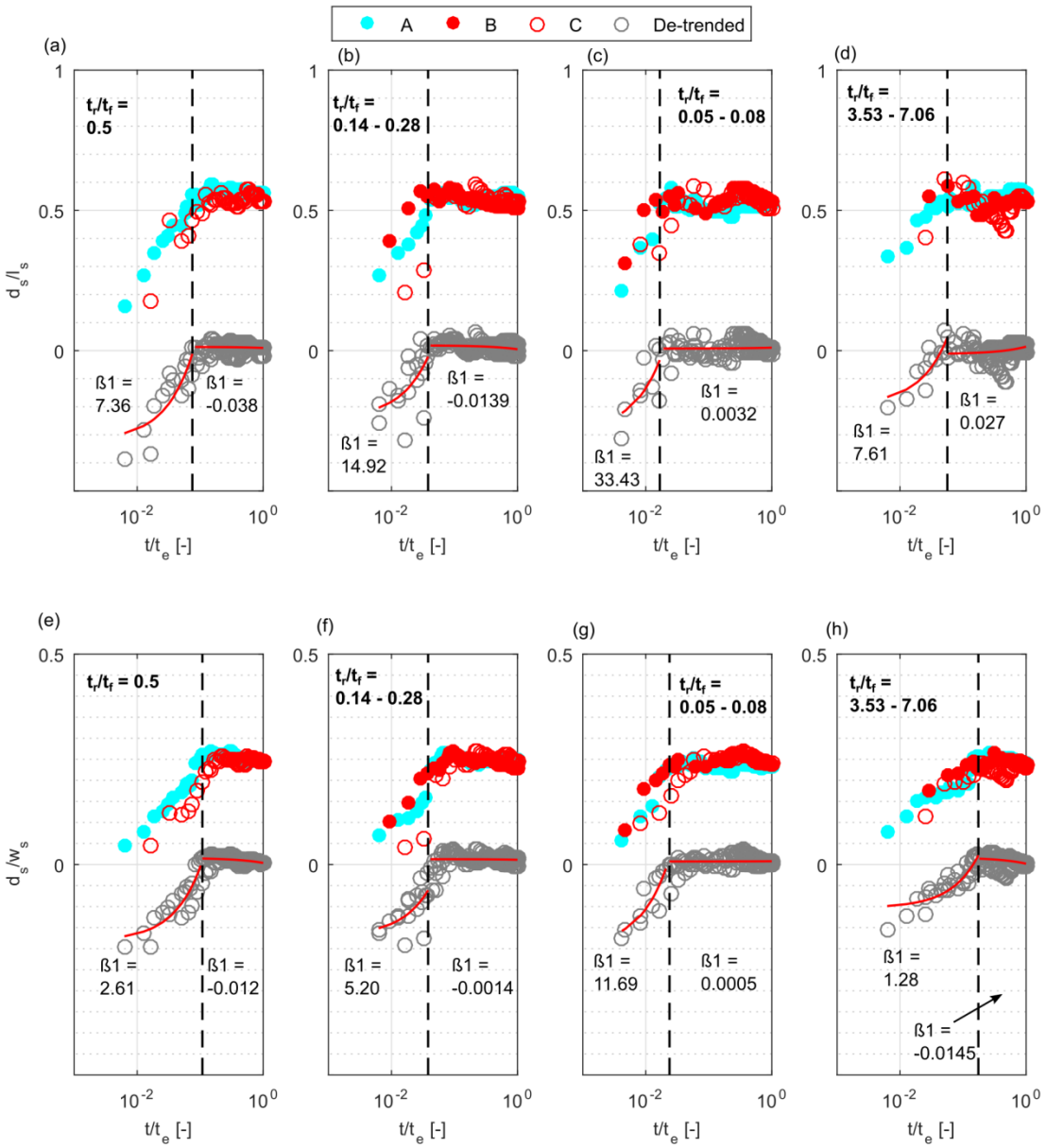

Figure 7. Geometrical relations of the local scour hole vs. non –dimensional time scale for $W_k = 1.70$ and different hydrograph shape of experimental series A, B, and C.

For a given W_k an irrespective of hydrograph shape the probability distribution of d_s/l_s and d_s/w_s within the bounds marked by the change points in time was estimated by kernel density estimation. For $W_k = 1.70$ at t/te 0.05,

0.10, respectively, d_s/l_s and d_s/w_s are characterized by a platokurtic (i.e. flat) distribution and more dispersed values while for $t/t_e > 0.05$, 0.10, respectively, d_s/l_s and d_s/w_s are characterized by a lepetokurtic distribution (i.e. sharply peaked) where values are closer to the mean (Figure 7a-b).

For $W_k = 2.46$ and 3.49 at t/t_e 0.05, 0.10, respectively, the distribution of d_s/l_s and d_s/w_s are moderate in breadth compared to $W_k = 1.70$ while for $t/t_e >$ 0.05, 0.10, respectively, the distributions are mesokurtic with a medium peaked height indicating (Figure 7c-f).

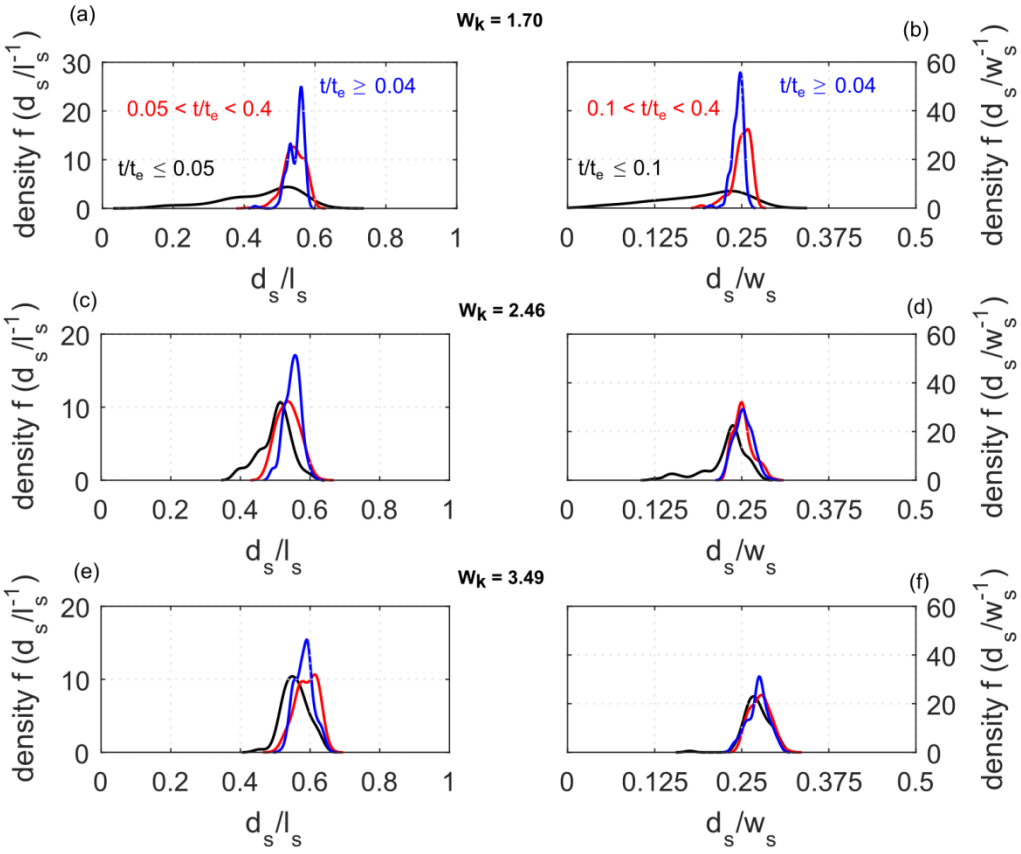

Figure 8. Kernel density estimation of d_s/l_s and d_s/w_s within the bounds of the estimated change points in time.

4. Interpretation and Discussion

4.1 Hydrograph Shape and Duration

The experimental results suggested that the hydrograph shape affected the time evolution of local scour holes at a boulder-like obstacle as d_s increased occurred mainly on the rising limb (t_r) of the hydrograph. Thus, it can be stated that

the steeper t_r (i.e. positive skewed) the quicker d_s, l_s, and w_s achieve sizes comparable to their final sizes for given hydraulic conditions. This observation coincides with experimental results on the time evolution of d_s at bridge piers during hydrographs (Chang et al. 2004; Salamatian et al. 2014). However, for the used boulder-like obstacle and the ephemeral (i.e. dry bed) conditions at the beginning of the experiments intense enlargement in d_s, l_s, and w_s occurred on the rising limb for relatively shallow flow conditions in which flow depth was comparable to the obstacle size (i.e. $d_w/L_o = 1$). The finding can be interpreted in the light of experimental hydraulic data presented in Schlömer et al. (2020) who have attributed the intense enlargement at d_w/L_o =1 to an intense downflow at the obstacle front and an efficient HV system at the base. With increasing d_w/L_o in course of the hydrograph this physical effect weakens as the obstacle becomes submerged ($d_w/L_o > 1.1$).

For the present data, the subsequent easing d_s-incision in time can be attributed to a weakening of the HV system that subsides into the local scour hole during depth-incision where it expands in diameter. The expansion decreases the shear stress beneath the vortex for sediment mobilization and induces equilibrium of depth-incision (Dargahi 1990; Unger & Hager 2006). Thus, local scour hole and HV system in time are connected via feedback loops indicating a self-organizing behavior (Coco & Murray 2007). This characteristic became pronounced due to the stepwise hydrographs considered in this study and the superposition of local scour hole evolution (López et al. 2014) while it also explains why no substantial d_s-incision occurred on t_f although the hydraulic boundary conditions on each step were equal to steps on t_r. According to Tubaldi et al., (2017) this highlights the history and time dependence of local scouring process in which memory effects (i.e. dependence on antecedent sizes of d_s, l_s, and w_s rather than on actual flow conditions) need to be considered (cf. Schlömer & Herget, 2021).

4.2 Flow Intensity

While hydrograph shape controlled the time evolution of local scouring, the flow work (W_k) exerted by the hydrograph and more specific the flow intensity (U_m/U_c) controlled the final sizes of d_s, l_s, and w_s which is also reported by (Link et al. 2017) for experimental data on d_s at bridge piers. Although for a given W_k, U_m/U_c was maximized at I_p of each hydrograph, the peak flow did not contribute to substantial enlargement of the scour hole at the boulder-like obstacle which is in disagreement to experimental observations reported for scouring at bridge piers during hydrographs (Gjunsburgs et al. 2010; Tabarestani & Zarrati 2017). However, the boulder-like obstacles were submerged ($d_w/L_o = 2.79$) at peak flow so that much of the approaching current flowed over the obstacle top so that a weaker downflow and HV persist at the obstacle base. This impact of d_w/L_o on the geometrical length scales of the local scour hole is documented in the experimental data presented by Schlömer et al. (2020a) in which the normalized local scour hole volume (i.e. $(d_s l_s w_s)^{1/3} L_o^{-1}$) for a given U_m/U_c is 60% smaller for $d_w/L_o > 2$ compared to d_w/L_o = 0.8-1.

Thus, opposite to bridge piers the impact I_p on local scour hole enlargement at

the submerged boulder-like obstacle is negligible while most of the final size of d_s, l_s, and w_s is attained on t_r prior to q_p, while for the live-bed hydrographs (Wk = 3.49) bed load mobilization at peak flow even cause an refilling of the local scour hole and an decrease in d_s, l_s, and w_s. Due to the absence of suspension refilling of the local scour hole did not occurred on the falling limb of the hydrographs which is commonly described local scour holes at the recessing stage of a flood (Link et al. 2020).

4.3 Geometrical Relation in Time

The enlargement of l_s and w_s was directly coupled to the incision of d_s on t_r so that two evolutionary stages of local scouring over time were identified based on d_s/l_s, and d_s/w_s that distinguish the beginning stage and maturing stage of scour incision. For W_k at clear-water condition ($U_m/U_c < 1$) the stages were present for all hydrograph shapes, although their temporal occurrence slightly varied. With increasing W_k and live-bed conditions the distinction of beginning and maturing stage based on d_s/l_s and d_s/w_s vanishes as in particular for the beginning phase of local scouring the geometrical relations were larger due higher U_m/U_c and intense enlargement.

The presence of two stages is attributed to the hydrodynamic evolution of the HV in course of local scouring that causes a stabilization in the erosive energy of the vortex and vice versa a significant reduction in further depth-incision (Rogers et al. 2020; Manes & Brocchini 2015). The present observation of different stage of local scouring corresponds to results reported in Schlömer (2020) for local scouring at boulder-like obstacles exposed to long lasting (t_e = 5760 min) constant discharge where substantial depth-incision occurred for t/t_e 0.04. However, due to the long duration of experiments they observed slight enlargement in w_s that resulted in a decreasing tendency of d_s/w_s beyond the aforementioned threshold in time. The enlargement of w_s was attributed to the convection of detached shear layers from the HV at the lateral sides of the obstacle that resulted in strong amplification of shear stress at the bed.

It is obvious that the enlargement of local scour holes at boulder-like obstacles occurs in a relatively short time period originating at the onset of local scouring irrespective of hydraulic condition (i.e. steady vs. unsteady discharge).

4.4 Shortcomings of Experimental Setup

The experimental runs were conducted at reduced complexity and neglected boundary conditions that impact local scouring but might be plausible at field condition. The boulder-like obstacle was mounted and prevented from tilting and into the local scour hole that is likely to occur during depth-incision irrespective of spatial scale (Rennie et al. 2017) (cf. Figure 1b). Obstacle tilting would incline the obstacle's frontal face and alter its exposure to flow which decelerates depth-incision and causes shallow local scour holes that are comparable long and wide. As a consequence deviations in d_s/l_s, and d_s/w_s irrespective of time are described (Schlömer et al. 2021).

For the present investigation rather simple shaped single peak hydrographs were constructed mainly due to the limited capability in adjusting discharge to more complex scenarios as described in Pizarro et al., (2017). However, the experiments revealed that substantial local scouring occurred on the rising limb (t_r) irrespective of the hydrograph shape while local scouring was mainly absent on the falling limb (t_f) as also reported by (Chang et al. 2004; Kothyari et al. 1992) for local scouring at emergent bridge piers.

Although the present experimental setup did consider live-bed conditions ($U_m/U_c > 1$) that impacted the size of the geometrical length scales by refilling processes, the flow intensity at peak flow ($U_m/U_c = 1.13$) is rather small compared to flow intensities likely to floods at natural conditions (U_m/U_c 20) (Ettmer et al. 2015; Link et al. 2017). However,

for the here considered case of a boulder-like obstacle an increased flow intensity might cause (a) an complete burial of the local scour hole due to the continuous sediment supply and the passage of bed forms; (b) a mobilization of the obstacle itself due to impulsive force that is directed from the high-pressure side of the frontal face towards the low-pressure wake and consequently lifts the obstacle (Alexander & Cooker 2016; Carling et al. 2010). Consequently, no scour hole would have formed.

5. Conclusion and Outlook

The time evolution of characteristic length scales of a local scour holes (i.e. depth, length, and width) emerging at a boulder-like obstacle exposed to stepped hydrographs of different shape, overall duration, and flow intensity was physically modelled in a process-focused laboratory flume study. Recalling the objectives formulated in the Introduction the findings of the present study can be summarized as follows:

1. Irrespective of the hydrograph shape intense depth-incision and enlargement in length and width of the local scour hole occurred on the rising limb in which on average 71% of the final sizes at the end of the experiments were reached in only 10% of the overall duration of the hydrographs. Within the considered time range of short duration hydrographs (120 min to 480 min) the overall duration of the hydrographs had marginal impact on the sizes of the geometrical length scales of the local scour holes. The submergence ratio of the obstacle is a primary control parameter for local scouring processes on the rising limb while the impact of peak flow is negligible if the obstacle is submerged so that the flow depth is > than the obstacle size. However, general bed load transport (i.e. live-bed condition) during the hydrographs and especially at the peak flow refilled the local scour holes and reduced the sizes depth, length, and width.

2. Irrespective of the hydrograph shape the enlargement of the local scour hole length and width in time is closely related to the depth-incision as the triggering process. Without general bed load transport (i.e. clear-water condition) during hydrographs two temporal stages are identified

based on the statistically modelling of geometrical relation of the scour hole (i.e. depth to length, and depth to width) in time that are consistent to prior observations on local scouring at long lasting constant discharge (cf. Schlömer et al., 2020b).

Although the experimental setup has simplified natural complexity, the evolution of the geometrical relations in time is relevant in course of a hydraulic interpretation of local scour holes at boulders at field conditions as scale invariance of processes and form in time enables transfer to larger spatial scale. Thus, it is speculated that the geometrical relation of preserved local scour holes at boulder obstacles located in ephemeral streams may be used as length scale to plausible estimate the minimum duration of the rising limb of a flood hydrograph. Due to a high uncertainty further analysis are needed, especially the impact of repeated hydrographs onto the geometry of local scour holes is required in this context (cf. Schlömer & Herget, 2021).

Open Research

The data presented here can be downloaded in tabular form on condition that we are acknowledged in any subsequent publication.

Acknowledgments

The present study was not financially supported.

References

Alexander, J, & Cooker, M. J. (2016): Moving boulders in flash floods and estimating flow conditions using boulders in ancient deposits. Sedimentology 63 (6), 1582–1595, https://doi.org/10.1111/sed.12274

Baynes, E R.C., van de Lageweg, W. I., McLelland, S. J., Parsons, D. R., Aberle, J., Dijkstra, J. et al. (2018): Beyond equilibrium: Re-evaluating physical modelling of fluvial systems to represent climate changes. *Earth-Science Reviews* 181, 82–97, https://doi.org/10.1016/j.earscirev.2018.04.007

Bergeron, N. E., & Abrahams, A. D. (1992): Estimating shear velocity and roughness length from velocity profiles. *Water Resources Research* 28 (8), 2155–2158, https://doi.org/10.1029/92WR00897

Bombar, G. (2020): Scour Evolution Around Bridge Piers Under Hydrographs with High Unsteadiness. *Iranian Journal of Science and Technology Transactions of Civil Engineering* 44 (1), 325–337, https://doi.org/10.1007/s40996-019-00321-8

Breusers, H. N. C., & Raudkivi, A. J. (1991): *Scouring* (Hydraulic structures design manual, 2) Rotterdam: Balkema

Camarasa-Belmonte, A M., & Segura, F- (2001): Flood events in Mediterranean ephemeral streams (ramblas) in Valencia region, Spain. *CATENA* 45 (3), 229–249, https://doi.org/10.1016/S0341-8162(01)00146-1

Carling, P. A., Hoffmann, M., Blatter, A. S. (2010): Initial Motion of Boulders in Bedrock Channels. In P. K. House, R.H. Webb, V.R. Baker, D.R. Levish (Eds), *Ancient floods, modern hazards. Principles and applications of paleoflood hydrology* (Water Science and Application 5, pp. 147–160). Washington, DC: American Geophysical Union

Chang, W.-Y., Lai, J.-S., Yen, C.-L. (2004): Evolution of Scour Depth at Circular Bridge Piers. *Journal of Hydraulic Engineering*130 (9), 905–913, https://doi.org/10.1061/(ASCE)0733-9429(2004)130:9(905)

Chen, Y., Yang, Z., Wu, H. (2019): Evolution of Turbulent Horseshoe Vortex System in Front of a Vertical Circular Cylinder in Open Channel. *Water* 11 (10), 2079, https://doi.org/10.3390/w11102079

Chen, Q., Qi, M., Zhong, Q., Li, D. (2017): Experimental study on the multimodal dynamics of the turbulent horseshoe vortex system around a circular cylinder. *Physics of Fluids* 29 (1), 15106, https://doi.org/10.1063/1.4974523

Chiew, Y.-M. (1995): Mechanics of Riprap Failure at Bridge Piers. *Journal of Hydraulic Engineering*121 (9), 635–643, https://doi.org/10.1061/(ASCE)0733-9429(1995)121:9(635)

Coco, G., & Murray, A. B. (2007): Patterns in the sand: From forcing templates to self-organization. *Geomorphology* 91 (3-4), 271–290, https://doi.org/10.1016/j.geomorph.2007.04.023

Collischonn, W., Fleischmann, A., Paiva, R. C. D., Mejia, A. (2017): Hydraulic Causes for Basin Hydrograph Skewness. *Water Resources Research*53 (12), 10603–10618, https://doi.org/10.1002/2017WR021543

Dargahi, B. (1990): Controlling Mechanism of Local Scouring. *Journal of Hydraulic Engineering*116 (10), 1197–1214, https://doi.org/10.1061/(ASCE)0733-9429(1990)116:10(1197)

Escauriaza, C., & Sotiropoulos, F. (2011): Initial stages of erosion and bed form development in a turbulent flow around a cylindrical pier. *Journal of Geophysical Research* 116 (F3), 671, https://doi.org/10.1029/2010JF001749

Ettema, R., Constantinescu, G., Melville, B. (2011): *Evaluation of Bridge Scour Research: Pier Scour Processes and Predictions*. Washington, D.C.: Transportation Research Board.

Ettmer, B., Orth, F., Link, O. (2015): Live-Bed Scour at Bridge Piers in a Lightweight Polystyrene Bed. *Journal of Hydraulic Engineering*141 (9), 4015017, https://doi.org/10.1061/(ASCE)HY.1943-7900.0001025

Euler, Th., & Herget, J. (2012): Controls on local scour and deposition induced by obstacles in fluvial environments. *CATENA* 91, 35–46, https://doi.org/10.1016/j.catena.2010.11.002

Euler, Th., Herget, J., Schlömer, O., Benito, G. (2017): Hydromorphological processes at submerged solitary boulder obstacles in streams. *CATENA* 157, 250–267, https://doi.org/10.1016/j.catena.2017.05.028

Gjunsburgs, B., Jaudzems, G., Govša, J. (2010): Hydrograph Shape Impact on the Scour Development with Time at Engineering Structures in River Flow. *Construction Science* 11, 6–12

Hager, W. H., & Hutter, K. (1984): On pseudo-uniform flow in open channel hydraulics. *Acta Mechanica* 53 (3-4), 183–200, https://doi.org/10.1007/BF01177950

Hager, W. H., Unger, J. (2010): Bridge Pier Scour under Flood Waves. *Journal of Hydraulic Engineering*136 (10), 842–847, https://doi.org/10.1061/(ASCE)HY.1943-7900.0000281

Herget, J., Euler, Th., Roggenkamp, Th., Zemke, J. (2013): Obstacle marks as palaeohydraulic indicators of Pleistocene megafloods. *Hydrology Research* 44 (2), 300–317, https://doi.org/10.2166/nh.2012.155

Herget, J., Schütte, F., Klosterhalfen, A. (2015): Empirical modelling of outburst flood hydrographs. *Zeitschrift für Geomorphologie Supplementary Issues* 59 (3), 177–198, https://doi.org/10.1127/zfg_suppl/2015/S-59224

Hong, J.-H., Chiew, Y.-M., Yeh, P.-H., Chan, H.-C. (2017): Evolution of Local Pier-Scour Depth with Dune Migration in Subcritical Flow Conditions. *Journal of Hydraulic Engineering*143 (4), 4016098, https://doi.org/10.1061/(ASCE)HY.1943-7900.0001261

Killick, R., Fearnhead, P., Eckley, I. A. (2012): Optimal Detection of Changepoints With a Linear Computational Cost. *Journal of the American Statistical Association* 107 (500), 1590–1598, https://doi.org/10.1080/01621459.2012.737745

Kirkil, G., Constantinescu, G. (2010): Flow and turbulence structure around an in-stream rectangular cylinder with scour hole. *Water Resources Research* 46 (11), https://doi.org/10.1029/2010WR009336

Kothyari, U. C., Garde, R. C. J. Kittur G. R. R. (1992): Temporal Variation of Scour Around Circular Bridge Piers. *Journal of Hydraulic Engineering118* (8), 1091–1106, https://doi.org/10.1061/(ASCE)0733-9429(1992)118:8(1091)

Lee, S. O., & Sturm, T. W. (2009): Effect of Sediment Size Scaling on Physical Modeling of Bridge Pier Scour. *Journal of Hydraulic Engineering*135 (10), 793–802, https://doi.org/10.1061/(ASCE)HY.1943-7900.0000091

Li, J., Qi, M., Fuhrman, D. R., Chen, Q. (2018): Influence of turbulent horseshoe vortex and associated bed shear stress on sediment transport in front of a cylinder. *Experimental Thermal and Fluid Science* 97, 444–457, https://doi.org/10.1016/j.expthermflusci.2018.05.008

Link, O., Castillo, C., Pizarro, A., Rojas, A., Ettmer, B., Escauriaza, C., Manfreda, S. (2017): A model of bridge pier scour during flood waves. *Journal of Hydraulic Research* 55 (3), 310–323, https://doi.org/10.1080/00221686.2016.1252802

Link, O., García, M., Pizarro, A., Alcayaga, H., Palma, S. (2020): Local Scour and Sediment Deposition at Bridge Piers during Floods. *Journal of Hydraulic Engineering146* (3), 4020003, https://doi.org/10.1061/(ASCE)HY.1943-7900.0001696

Link, O., González, C., Maldonado, M., Escauriaza, C. (2012): Coherent structure dynamics and sediment particle motion around a cylindrical pier in developing scour holes. *Acta Geophysica.* 60 (6), 1689–1719, https://doi.org/10.2478/s11600-012-0068-y

López, G., Teixeira, L., Ortega-Sánchez, M., Simarro, G. (2014): Estimating Final Scour Depth under Clear-Water Flood Waves. *Journal of Hydraulic Engineering* 140 (3), 328–332, https://doi.org/10.1061/(ASCE)HY.1943-7900.0000804

Manes, C., & Brocchini, M. (2015): Local scour around structures and the phenomenology of turbulence. *Journal of Fluid Mechanics* 779, 309–324, https://doi.org/10.1017/jfm.2015.389

Manes, C., Coscarella, F., Rogers, A., Gaudio, R. (2018): Viscosity effects on local scour around vertical structures in clear-water conditions. *E3S Web of Conferences.* 40, 3038, https://doi.org/10.1051/e3sconf/20184003038.

Manfreda, S., Link, O., Pizarro, A. (2018): A Theoretically Derived Probability Distribution of Scour. *Water* 10 (11), 1520, https://doi.org/10.3390/w10111520

Mao, L. (2012): The effect of hydrographs on bed load transport and bed sediment spatial arrangement. Journal of Geophysical Research 117 (F3), https://doi.org/10.1029/2012JF002428

Melville, B. W., & Chiew, Y.-M. (1999): Time Scale for Local Scour at Bridge Piers. *Journal of Hydraulic Engineering*125 (1), 59–65, https://doi.org/10.1061/(ASCE)0733-9429(1999)125:1(59)

Melville, B. W., Coleman, S. E. (2000): *Bridge scour.* Highlands Ranch, Colorado: Water Resources Publication.

Nakagawa, H., & Nezu, I. (1993): *Turbulence in Open Channel Flows*, Rotterdam: CRC Press.

Oliveto, G., & Hager, W. H. (2002): Temporal Evolution of Clear-Water Pier and Abutment Scour. *Journal of Hydraulic Engineering128* (9), 811–820, https://doi.org/10.1061/(ASCE)0733-9429(2002)128:9(811)

Papanicolaou, A. N., Tsakiris A.G., Kramer C.M. (2010): Effects of relative submergence on flow and sediment patterns around clasts. In *River Flow 2010 (pp.* 793–799). Karlsruhe, Germany: Bundesanstalt für Wasserbau.

Pizarro A., Tubaldi E. (2019): Quantification of Modelling Uncertainties in Bridge Scour Risk Assessment under Multiple Flood Events. *Geosciences* 9 (10), 445, https://doi.org/10.3390/geosciences9100445

Pizarro, A., Ettmer, B., Manfreda, S., Rojas, A., Link, O. (2017): Dimensionless Effective Flow Work for Estimation of Pier Scour Caused by Flood Waves. *Journal of Hydraulic Engineering*143 (7), 6017006, https://doi.org/10.1061/(ASCE)HY.1943-7900.0001295

Pizarro, A., Manfreda, S., Tubaldi, E. (2020): The Science behind Scour at Bridge Foundations: A Review. *Water* 12 (2), 374, https://doi.org/10.3390/w12020374

Powell, D. M. (2009): Dryland rivers: processes and forms. In A.J. Parsons & A D. Abrahams (Eds.): *Geomorphology of Desert Environments* (pp. 333-373). Dordrecht: Springer.

Radice, A., Porta, G., Franzetti, S. (2009): Analysis of the time-averaged properties of sediment motion in a local scour process. *Water Resources Research* 45 (3), https://doi.org/10.1029/2007WR006754

Radice, A., & Tran, C. K. (2012): Study of sediment motion in scour hole of a circular pier. *Journal of Hydraulic Research* 50 (1), 44–51, https://doi.org/10.1080/00221686.2011.641764

Reid, I., Laronne, J. B., Powell, D. M. (1998): Flash-flood and bedload dynamics of desert gravel-bed streams. *Hydrological Processes* 12 (4), 543–557, https://doi.org/10.1002/(SICI)1099-1085(19980330)12:4<543::AID-HYP593>3.0.CO,2-C

Rennie, S. E., Brandt, A., Friedrichs, C. T. (2017): Initiation of motion and scour burial of objects underwater. *Ocean Engineering* 131, 282–294, https://doi.org/10.1016/j.oceaneng.2016.12.029

Rodríguez-Iturbe, I., Valdés, J. B. (1979): The geomorphologic structure of hydrologic response. *Water Resources Research* 15 (6), 1409–1420, https://doi.org/10.1029/WR015i006p01409

Rogers, A., Manes, C., Tsuzaki, T. (2020): Measuring the geometry of a developing scour hole in clear-water conditions using underwater sonar scanning. *International Journal of Sediment Research* 35 (1), 105–114, https://doi.org/10.1016/j.ijsrc.2019.07.005

Rushmer, E. L (2007): Physical-scale modelling of jökulhlaups (glacial outburst floods) with contrasting hydrograph shapes. *Earth Surface Processes and Landforms* 32 (6), 954–963, https://doi.org/10.1002/esp.1461

Salamatian, A., Tabarestani, M. K., Zarrati, A. R. (2014): Local scour at cylindrical bridge pier under a flood wave. In *River Flow 2014* (pp. 1387–1391) Leiden: CRC Press.

Schlömer, Oliver (2020): Morphodynamic relation of obstacle marks at boulder-like obstructions in time. In *River Flow 2020.* (pp. 719-727) Leiden: CRC

Press.

Schlömer, O., Herget, J., Euler, Th. (2020): Boundary condition control of fluvial obstacle mark formation – framework from a geoscientific perspective. Earth Surface Processes and Landforms 45 (1), 189–206, https://doi.org/10.1002/esp.4793

Schlömer, O., Grams, P. E., Buscombe, D., Herget, J. (2021): Geometry of obstacle marks at instream boulders – integration of laboratory investigations and field observations. Earth Surface Processes and Landforms 46 (3), 659679, https://doi.org/10.1002/esp.5055

Schlömer, O. & Herget, J. (2021): Flume experiments on the geometry of local scour holes at boulder-like obstacles during unsteady flow: Part II – Enlargement Processes and the Impact of Hydrograph Chronology (submitted to WRR)

Shamloo, H., Rajaratnam, N., Katopodis, C. (2001): Hydraulics of simple habitat structures. Journal of Hydraulic Research 39 (4), 351–366, https://doi.org/10.1080/00221680109499840

Sheppard, D. M., & Miller, W. (2006): Live-Bed Local Pier Scour Experiments. *Journal of Hydraulic Engineering*132 (7), 635–642, https://doi.org/10.1061/(ASCE)0733-9429(2006)132:7(635)

Simarro, G., Fael, C. M. S., Cardoso, A. H. (2011): Estimating Equilibrium Scour Depth at Cylindrical Piers in Experimental Studies. *Journal of Hydraulic Engineering* 137 (9), 1089–1093, https://doi.org/10.1061/(ASCE)HY.1943-7900.0000410

Simarro, G., Teixeira, L., Cardoso, A. H. (2007): Flow Intensity Parameter in Pier Scour Experiments. *Journal of Hydraulic Engineering133* (11), 1261–1264, https://doi.org/10.1061/(ASCE)0733-9429(2007)133:11(1261)

Tabarestani, M. K., Zarrati, A. R. (2017): Local scour calculation around bridge pier during flood event. *KSCE Journal of Civil Engineering* 21 (4), 1462–1472, https://doi.org/10.1007/s12205-016-0986-3

Tubaldi, E., Macorini, L., Izzuddin, B. A., Manes, C., Laio, F. (2017): A framework for probabilistic assessment of clear-water scour around bridge piers. *Structural Safety* 69, 11–22, https://doi.org/10.1016/j.strusafe.2017.07.001

Unger, J., & Hager, W. H. (2006): Down-flow and horseshoe vortex characteristics of sediment embedded bridge piers. *Experiments in Fluids* 42 (1), 1–19, https://doi.org/10.1007/s00348-006-0209-7

Waters, K. A., & Curran, J (2015): Linking bed morphology changes of two sediment mixtures to sediment transport predictions in unsteady flows. *Water Resources Research* 51 (4), 2724–2741, https://doi.org/10.1002/2014WR016083

Williams, P., Balachandar, R., Bolisetti, T. (2019): Examination of Blockage Effects on the Progression of Local Scour around a Circular Cylinder. *Water* 11 (12), 2631, https://doi.org/10.3390/w11122631